Bulletin of Geophysics and Oceanography Vol. 62, n. 3, pp. 513-526; September 2021
DOI 10.4430/bgo00351

New geodetic constraints to reveal seismic potential of central Marmara region, Turkey

H.H. Yavasoglu[1], I. Tiryakioglu[2], M.F. Karabulut[3], E.E. Eyubagil[2], A. Ozkan[1], F. Masson[4], E. Klein[5], V.E. Gulal[3,7], R.M. Alkan[1], M.N. Alkan[6], M. Isiler[1] and A.E. Arslan[1]

[1] *Geomatic Eng. Dept., ITU, Maslak, Istanbul, Turkey*
[2] *Geomatic Eng. Dept., Afyon Kocatepe University, Afyonkarahisar, Turkey*
[3] *Geomatic Eng. Dept., Yildiz Tech. University, Esenler, Istanbul, Turkey*
[4] *IPG, UMR 7516, Université de Strasbourg/EOST CNRS, Strasbourg, France*
[5] *Laboratoire de Géologie, ENS, CNRS UMR8538, Paris 05, Île-de-France, France*
[6] *Hitit University, Osmancık, Corum, Turkey*
[7] *Kagithane, Atlas University, Istanbul, Turkey*

(Received: 20 April 2020; accepted: 22 December 2020; published online: 20 September 2021)

ABSTRACT The North Anatolian Fault (NAF) is a fault zone that produced destructive earthquakes (Erzincan 1939 and 1992, Ladik 1943, Gerede 1944, Duzce 1999, Izmit 1999) in the last century. After this destructive earthquake migration, it is forecasted that the next seismic event on the NAF could be in the western part of the fault, which passes through the Marmara region. Due to the possibility of an earthquake in Istanbul, the most crowded and historical city in Turkey, researchers have increasingly paid attention to the western segment of the NAF within the Marmara Sea since the 1999 earthquakes. Many scientists from different disciplines such as geodesy, geology, geophysics, etc. have been trying to understand this phenomenon. However, it is understood from the literature that a comprehensive geodetic study is crucial to constrain the NAF segment between Istanbul and Tekirdağ provinces. Therefore, we created a new network consisting of continuous GPS stations with 10-km interdistances along the shoreline, which was integrated with existing GNSS networks in the Marmara region. Data acquisition was carried out between August 2017 and February 2020. In this study, preliminary results obtained from the integration of the newly established network with the other GNSS networks are presented.

Key words: geodesy, deformation, NAF, tectonics.

1. Introduction

The North Anatolian Fault (NAF) is a major destructive, seismically active and continental strike-slip fault, extending from the Bingol province in the east, to the Saros Gulf, west Turkey (Ketin, 1948; McKenzie, 1972; Jackson and McKenzie, 1984; Barka, 1992, 1996; Şengör *et al.*, 2004). It has a slip rate of about 24 mm/year (McClusky *et al.*, 2000; Reilinger *et al.*, 2006) with right-lateral characteristics according to the relative motion between Eurasian and Anatolian plates. The eastern and central sections of the NAF have mostly pure strike-slip motion (Aktuğ *et al.*, 2009, 2015; Özener *et al.*, 2010; Yavaşoğlu *et al.*, 2011; Tatar *et al.*, 2012; Ozdemir and

© 2021 - OGS

Karslıoğlu, 2019), despite the fact that the western part of the fault has its own complexities such as the Ismetpasa, Erdek, and Marmara segments (Ambraseys, 1970; Çakır *et al.*, 2005; Kutoglu *et al.*, 2008; Emre *et al.*, 2013; Kaneko *et al.*, 2013). In the last century, the NAF had an intense destructive seismic activity that began in 1939 in Erzincan, M_w = 7.9, and ended in 1999 in eastern Marmara, İzmit M_w = 7.4 and Duzce M_w = 7.1.

In earlier years, destructive earthquakes in the Marmara region occurred in 1509 on the Cinarcik segment (Yaltırak, 2002; Bulut *et al.*, 2019), in 1766 on the central part of the northern branch of the NAF (Ambraseys, 2002; Armijo *et al.*, 2002), again in 1766 on the Tekirdağ segment (Bulut *et al.*, 2019), and in 1912 on the Sarkoy-Murefte segment (Aksoy, 2009; Meghraoui *et al.*, 2012; Le Pichon *et al.*, 2014).

Apart from these destructive earthquakes, seismic activities with an instrumental magnitude of 4.8 and 5.8 were also recorded on 24 and 26 September 2019 in the Marmara Sea close to Marmaraereglisi and Silivri offshore (Istanbul), respectively. The focal depths of these earthquakes were about 10 km, which can be considered as shallow-focused. The September 2019 earthquakes, which primarily affected the Istanbul provinces and districts, were felt in almost the whole Marmara region (KOERI, 2019). According to moment-tensor solutions, the mechanism for these earthquakes is composed of both strike-slip and thrust components (KOERI, 2019).

Considering the seismic cycle of the NAF in the Marmara region, the next possible seismic event(s) may occur within a short duration (Şengör *et al.*, 2004). Thus, scientists from all over the world have focused on the Marmara segment of the NAF (hereafter, CiS for Cinarcik Segment, KS for Kumburgaz Segment, CeS for Central Segment, and TS for Tekirdağ Segment) in terms of geological, geodetic, seismic, geophysical, and tectonic aspects after the 1999 seismic activity (McClusky *et al.*, 2000; Nyst and Thatcher, 2004; Reilinger *et al.*, 2006; Aktuğ *et al.*, 2009, 2015; Floyd *et al.*, 2010; Özener *et al.*, 2010; Yavaşoğlu *et al.*, 2011; Ozdemir and Karslıoğlu, 2019).

Although studies have found similar results for the eastern and western parts of the NAF in the Marmara Sea, there are still divisions among researchers about the mid-segments of the NAF, especially the CeS and KS segments (Fig. 1). The integration of data acquired from bathymetric, seismological, geophysical, geodetic, and geological studies reveals the segments of the NAF in the Marmara Sea (Fig. 1) (Ergintav *et al.*, 2014; Schmittbuhl *et al.*, 2016; Klein *et al.*, 2017; Bulut *et al.*, 2019).

Klein *et al.* (2017) found that the geodetic constraints for the controversial segments (CeS and KS) in the midsections of the NAF in the Marmara Sea have considerable importance to resolve concerns. For this reason, it became clear that more geodetic data are needed between the western part of Istanbul and Tekirdağ in order to better understand the mechanism of these segments.

In this study, explanations are given on how a new geodetic network was established in order to monitor the strain accumulations across the NAF in the Marmara region and to enhance sparse geodetic data by installing seven new continuous GPS (cGPS) stations on the shoreline between the western part of Istanbul and Tekirdağ. In addition, the network design presented in our study was shown to be appropriate to monitor the deformations of the NAF in the central Marmara region. In particular, we sought to reveal the characteristics of deformations arising from the 24 and 26 September 2019 earthquakes.

While evaluating the initial results obtained with the integration of our newly generated network into the existing GNSS networks, we also attempted to determine the main reasons for the seismic gap on the CeS and KS seen in the SF4 and SF5 studies in Fig. 1. Secondly, we also sought to explain why there is no deformation on Profile-C given in SF2 (abbreviations from SF1 to SF5 are given in Fig. 1).

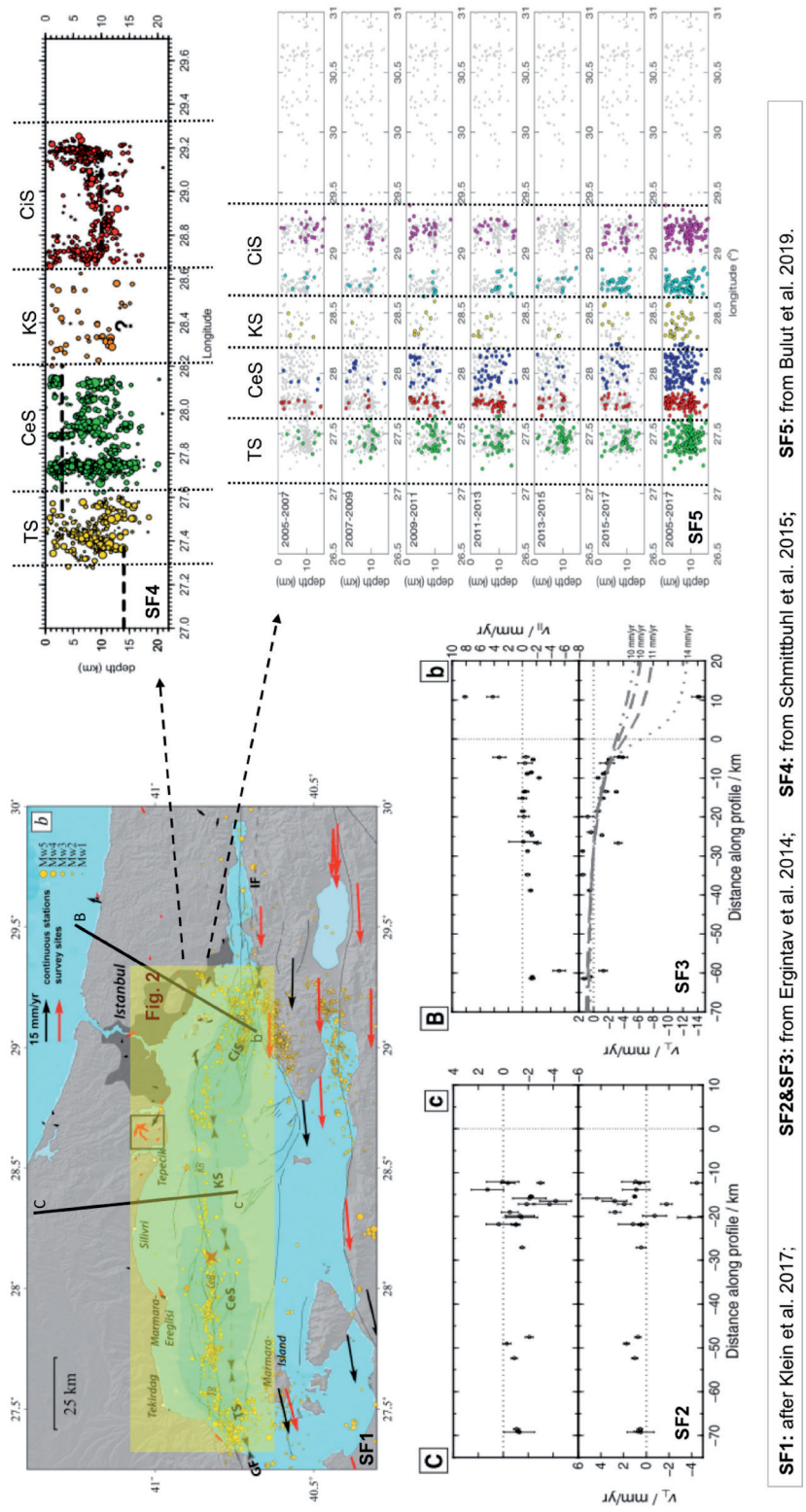


Fig. 1 - The study area (SF1), geodetic (SF1, SF2, and SF3) and seismic (SF4 and SF5) data obtained from previous studies. References for these studies are given in the figure.

The evaluation of the subgraphs given in Fig. 1 reveals the importance of our study. SF1 is the representation of geodetic data shown in Klein *et al.* (2017). SF2 and SF3 are generated from the geodetic data of Ergintav *et al.* (2014). SF2 and SF3 indicate the fault normal velocities obtained along the profiles perpendicular to the fault segment. In this context, profile B, with significant results, is shown by SF3. As stated in Ergintav *et al.* (2014), SF2 does not indicate any significant anomalies on profile C. Since the model structure did not change according to profile B, it could be said that the geodetic data in the region are insufficient along profile C. SF4 and SF5 represent the distribution of seismic data around the NAF in the Marmara region. It was demonstrated (Schmittbuhl *et al.*, 2015; Bulut *et al.*, 2019) that seismic activities on KS are relatively sparse compared to the other segments and the focal depths of seismic activity on TS, CeS, and CiS change remarkably. All these unclear points related to the topic indicate that detailed studies about these sequential segments (CiS, KS, CeS, and TS) in the central Marmara region are crucial. Therefore, it is highly important to investigate the possible reasons for this phenomenon in detail; hence, any scientific data supporting the resolution of this issue are valuable.

2. Geodetic data

To better understand the mechanism (two main behaviours; locked or aseismic creep) of the fault zones, one of the most suitable and economical tools is geodetic data obtained from GNSS/GPS and InSAR techniques to determine the surface deformations during the interseismic period. However, this is not the case for all segments of the NAF in the Marmara region since most sections of the NAF are within the Marmara Sea. Therefore, the common approach using conventional geodetic techniques is not an appropriate strategy for such kind of surface deformation monitoring. In this case, Klein *et al.* (2017) argued for the design of a geodetic network as close as possible to the NAF in the central Marmara region. To overcome this issue, the new stations in our geodetic network were arranged with almost uniform interdistances along the shoreline between Istanbul and Tekirdağ provinces in order to obtain the desired geodetic data set. Ultimately, after successful implementation of the new installations, all the cGPS stations within our geodetic network began simultaneously logging data in August 2017. Fortunately, the operation of the network continued without any considerably significant seismic activity until February 2020.

According to the predefined geodetic model (Klein *et al.*, 2017), seven new cGPS stations were established about every 10 km along the shoreline of the region from west of Istanbul (Tepecik/Beylikdüzü) to west of Tekirdağ (Uçmakdere) (Figs. 2a and 2b). The construction of each station consists of an aluminium mast fitted with a custom antenna mount, which is bolted onto rooftops with expansion bolts. These stations were located as far away as possible from settlements to allow long-term observations without being affected by local ground deformations. However, aside from site location, there are many other requirements that must be fulfilled for cGPS stations within a dynamic GNSS network. One of the most important requirements is an uninterruptible power supply for continuous data logging. The power for our equipment is supplied by the building grid power. The sky visibility from cGPS station antennas was complied with no obstructions above 5 degrees over the horizon. The multipath problem was overcome by avoiding reflective surfaces around the stations. The Internet infrastructure in the buildings allows for fast data transfer and remote connection to the station. There is always a trade-off between security and access in such facilities since the stations need to be kept safe from vandalism but also maintenance and inspection visits may be required without any bureaucratic restrictions.

Additionally, these newly installed stations were equipped with Trimble NetRS GNSS receiver and Trimble Zephyr Geodetic GNSS L1/L2 antenna sets. The accuracy of the NetRS receivers during static observations is ±5 mm + 0.5 ppm horizontal RMS with ±5 mm + 1 ppm vertical RMS. The acquisition settings are presented in Table 1. The new cGPS stations are labelled KHAS, GRAJ, DRA1, YENI, MOSQ, and NKUN as shown in Fig. 2, while the existing stations in the region, also shown in Fig. 2, were reconfigured (connected to 24 h electricity, increased memory card capacity, access to Internet infrastructure, etc) and included in our network.

Table 1 - Acquisition settings for the NetRS GNSS receivers.

Parameters	Acquisition Settings
Elevation Mask	0°
Sampling Interval	30 seconds
Session Length	1440 minutes (24-hour files)
System Name	Site's 4-character ID
Raw Data Format	T00/T01
File Naming	[System Name] + [Year] + [Month] + [Day] + [Start Time] + [Session ID]

In addition to these 7 new cGPS stations, a total of 40 pre-installed cGPS stations around the Marmara region were incorporated into our geodetic network. The GNSS data set, covering more than two years (August 2017 - February 2020) provided by 47 cGPS stations, was, then, processed with GAMIT/GLOBK software (Herring *et al.*, 2010). The processed network can be obtained from the horizontal velocity field of the Marmara region shown in the map subsequently. In the data processing and modelling, the surface deformation signal in the long term can have either linear, periodic, irregular, or episodic patterns, depending on the noise characteristics of the data set. By contrast, short-term signals derived from a complicated and high frequency data stack can provide information about the temporal oscillations; namely, the seasonal ground subsidence and uplift arising from withdrawal of subsurface reservoirs (Çırmık *et al.*, 2016; Tiryakioğlu *et al.*, 2017). In this study, the cGPS data for both short and long-term signals were analysed.

To separate the pre-earthquake period from the post-earthquake seismic phases, we followed a straightforward processing strategy for the analysis of the geodetic data in this study. First, for the inter-seismic period, the time series for station coordinates were obtained from the GAMIT/GLOBK processing using the data acquisition between August 2017 and September 2019 (before the 24 and 26 September 2019 earthquakes). Second, the daily estimates of station positions starting from September 2019 to February 2020 were attained to determine the co-seismic and post-seismic deformation signals. GAMIT processes were carried out with the same parameters for both stages of the analysis.

Most of the processing parameters in our analysis have common values that can be found from the following studies in the literature (Tiryakioğlu, 2013; Tiryakioğlu *et al.*, 2013, 2015, 2017, 2018; Çırmık and Pamukçu, 2017; Poyraz *et al.*, 2019). The station coordinates, Earth orientation parameters, and zenith delay parameters of the atmosphere at each station were estimated by solving phase ambiguities in daily GAMIT solutions. The daily solutions were combined into the reference frame defined with 12 IGS (International GNSS Service) stations (Table 2) by applying Kalman filtering in the GLOBK stage. Finally, time series for each cGPS station were obtained considering the separation of pre- and post-earthquake periods (Fig. 3).

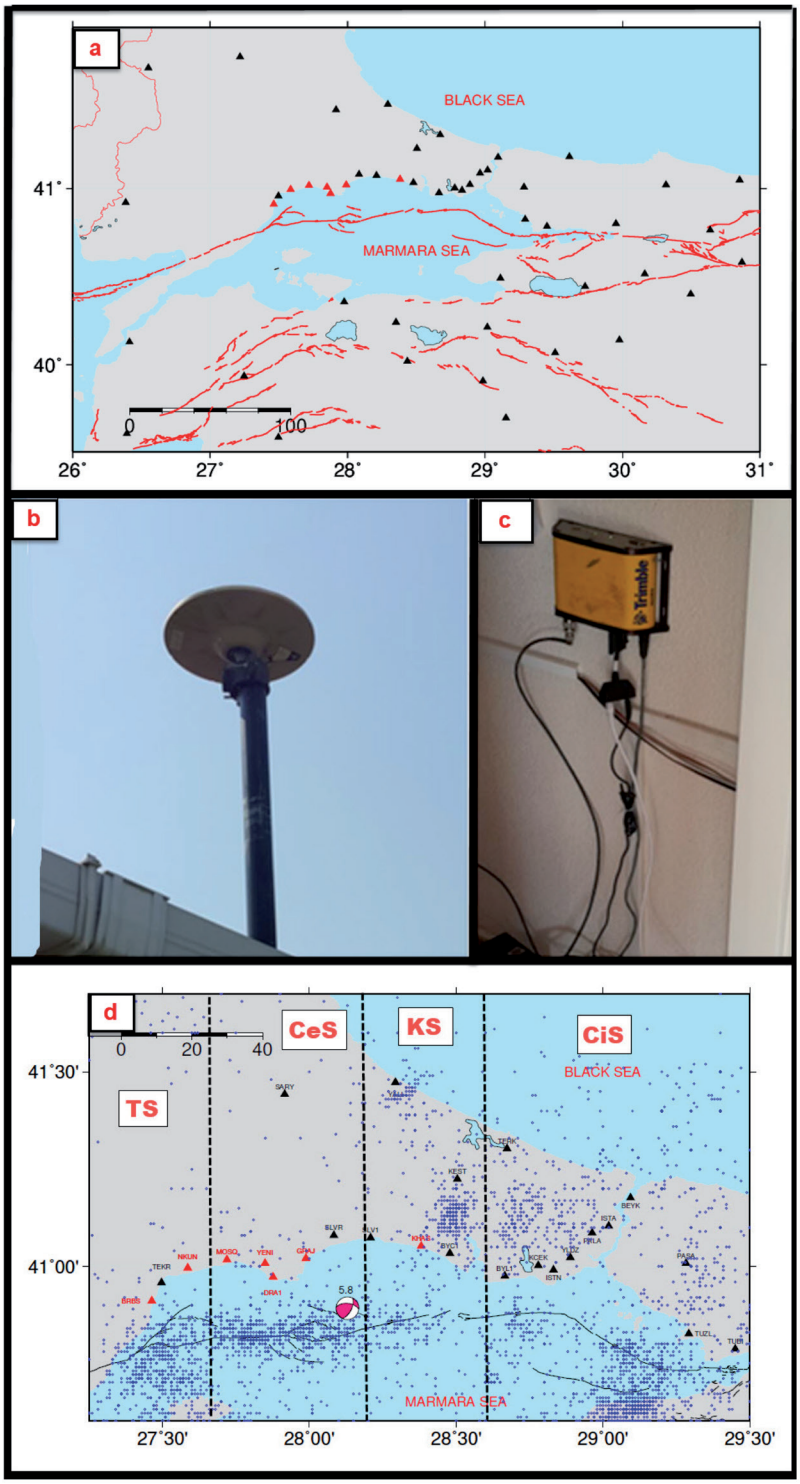


Fig. 2 - The entire processed network including all the new and existing stations (a); one of the newly-established cGPS stations (b and c), and faults depicted according to Le Pichon *et al.* (2003). Red triangles represent the 7 new cGPS stations, where black ones are the existing stations. The blue dots indicate seismic activities recorded by KOERI (www.koeri.boun.edu.tr/sismo/zeqdb). Abbreviations in the figure are given in the text. The focal mechanism represents the event occurring on 26 September 2019 (M_w = 5.8).

Although it seems that our geodetic network succeeded in differentiating the seismic phases according to the above-mentioned processing strategy, it is not easy to discuss the numerical results of the deformation caused by earthquakes since the magnitudes of the earthquakes were not large enough to cause any surface ruptures. In addition, it should be emphasised that the established geodetic network is designed to forecast the probable seismic activities that may occur in the region.

The horizontal velocity components for each cGPS station were estimated considering the data span for more than two years (from August 2017 to September 2019) according to the Eurasia fixed reference frame using a set of 9 IGS stations (Table 2). Frame realisation was carried out by applying constraints to the selected IGS stations for which both coordinates and velocities were precisely known. In order to realise the reference frame, the adjustments to the horizontal velocities of these selected IGS stations were minimised and the transformation parameters to ITRF2014 coordinates were hereby estimated. Reference frame realisation with the minimum of residuals was achieved by least-squares estimation applying constraints on both coordinates and velocities of the sites distributed in the Eurasia plate. Thus, the whole Marmara network was aligned to the ITRF network with the same reference epoch and all the velocities were derived in a Eurasia fixed reference frame. The post root mean square (RMS) value of the estimated velocity solution is 0.6 mm/yr after stabilisation with reference to the Eurasia plate (Fig. 4 and Table 2).

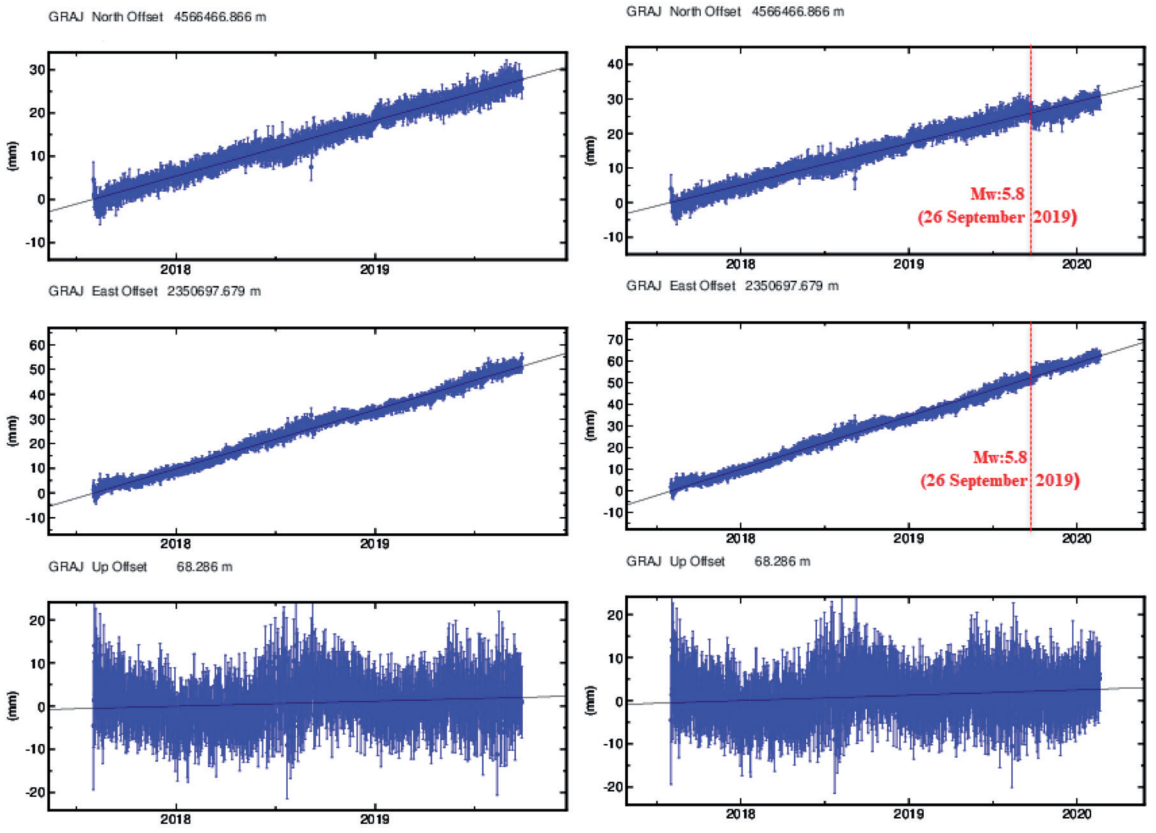


Fig. 3 - Time series for the GRAJ station: results of the processed data for August 2017 - August 2019 (left panels) and August 2017 - February 2020 (right panels).

Table 2 - Station velocities derived in a Eurasia - fixed reference frame (* IGS stations included in the velocity solution).

Station ID	Lon. (°)	Lat. (°)	First Obs.	Last Obs.	Ve (mm/year)	Vn (mm/year)	σVe (mm/year)	σVn (mm/year)
AYCK	26.39	39.61	2018.1	2019.2	-15.8	-14.4	1.1	1.2
BAN1	27.97	40.35	2016.8	2019.8	-19.1	-6.1	0.1	0.1
BEYK	29.09	41.18	2016.8	2019.8	-0.3	-2.5	0.1	0.1
BILE	29.98	40.14	2016.8	2019.8	-22.0	-4.1	0.1	0.1
BUSK	29.02	40.21	2016.8	2019.8	-20.5	-4.8	0.1	0.1
BYC1	28.48	41.03	2017.0	2018.3	0.2	-2.0	0.4	0.4
CNKL	26.41	40.13	2018.1	2018.9	-16.3	-10.0	1.1	1.3
DRCN	30.87	40.58	2018.0	2019.2	-16.8	-3.7	0.3	0.4
EDIR	26.55	41.68	2016.8	2019.8	2.2	-2.1	0.1	0.1
GMLK	29.11	40.49	2017.6	2019.8	-18.3	-2.9	0.2	0.2
HARM	29.15	39.68	2016.8	2019.8	-22.1	-6.2	0.2	0.2
HNDK	30.64	40.77	2018.3	2019.2	-6.1	0.9	0.3	0.3
IPS2	26.38	40.92	2018.3	2019.8	-1.6	-3.5	0.4	0.4
ISTA	29.02	41.10	2016.8	2019.8	-0.9	-1.8	0.1	0.1
ISTN	28.83	40.99	2016.8	2019.8	1.1	-2.0	0.1	0.1
IVRD	27.50	39.58	2018.1	2018.9	-11.5	-7.3	1.0	1.1
IZMT	29.95	40.80	2016.8	2019.8	-5.3	-1.8	0.1	0.1
IZNK	29.73	40.45	2018.5	2019.8	-19.9	-3.9	0.2	0.2
KCEK	28.78	41.00	2016.8	2019.8	-1.8	-1.7	0.1	0.1
KEST	28.50	41.23	2016.8	2019.8	0.8	0.7	0.1	0.1
KIRL	27.22	41.74	2016.8	2019.8	0.3	-1.9	0.1	0.1
KNRC	30.32	41.02	2018.1	2019.3	-0.1	-2.0	0.3	0.3
KOCL	30.85	41.05	2018.1	2019.3	-0.3	-1.5	0.3	0.3
KRCY	28.35	40.20	2017.6	2019.8	-19.9	-5.2	0.2	0.2
MKPS	28.43	40.02	2017.6	2019.8	-20.8	-6.6	0.2	0.2
NGL2	29.51	40.07	2018.6	2019.8	-21.9	-2.8	0.4	0.4
ORHN	28.98	39.91	2018.1	2019.8	-21.2	-5.9	0.2	0.3
PALA	28.96	41.09	2016.8	2019.8	-1.1	-1.6	0.1	0.1
PASA	29.28	41.01	2016.8	2019.8	-0.9	-1.2	0.2	0.2
PMKV	30.16	40.52	2018.1	2019.3	-19.7	-3.5	0.3	0.4
SARY	27.92	41.44	2016.8	2019.8	0.2	-2.0	0.1	0.2
SILE	29.61	41.18	2016.8	2019.8	0.1	-1.9	0.1	0.1
SLV1	28.21	41.07	2017.3	2018.8	-2.0	-1.9	0.4	0.4
SLVR	28.08	41.08	2016.8	2019.8	-0.4	-1.7	0.1	0.1
TEKR	27.50	40.96	2016.8	2019.8	-0.9	-3.6	0.1	0.1
TERK	28.67	41.30	2016.8	2019.8	0.1	-1.4	0.1	0.1
TRKL	30.50	40.40	2018.1	2019.3	-21.6	-4.3	0.3	0.4
TUBI	29.45	40.79	2016.8	2019.8	-5.1	-2.2	0.1	0.1
TUZL	29.29	40.83	2016.8	2019.8	-4.2	-1.7	0.1	0.1
YALI	28.29	41.47	2016.8	2019.6	0.2	-1.8	0.1	0.1
YLDZ	28.89	41.02	2016.8	2019.6	-0.8	-2.9	0.1	0.1
YNCE	27.25	39.93	2018.1	2018.9	-18.3	-6.4	1.0	1.2
CRAO *	33.99	44.41	2016.8	2019.8	0.8	-0.9	0.1	0.1
GLSV *	30.50	50.36	2016.8	2019.8	0.1	0.7	0.1	0.1
GRAZ *	15.49	47.07	2016.8	2019.8	-0.9	-0.2	0.1	0.1
NICO *	33.40	35.14	2016.8	2019.8	-0.7	-1.0	0.1	0.1
ORID *	20.79	41.13	2016.8	2019.8	-0.4	0.0	0.1	0.1
RAMO *	34.76	30.60	2016.8	2019.8	-0.4	-2.0	0.1	0.1
SOFI *	23.39	42.56	2016.8	2019.8	-0.2	-0.6	0.1	0.1
TELA *	34.78	32.07	2016.8	2019.8	-1.4	-1.4	0.1	0.1
WTZR *	12.88	49.14	2016.8	2019.8	-0.3	0.0	0.1	0.1

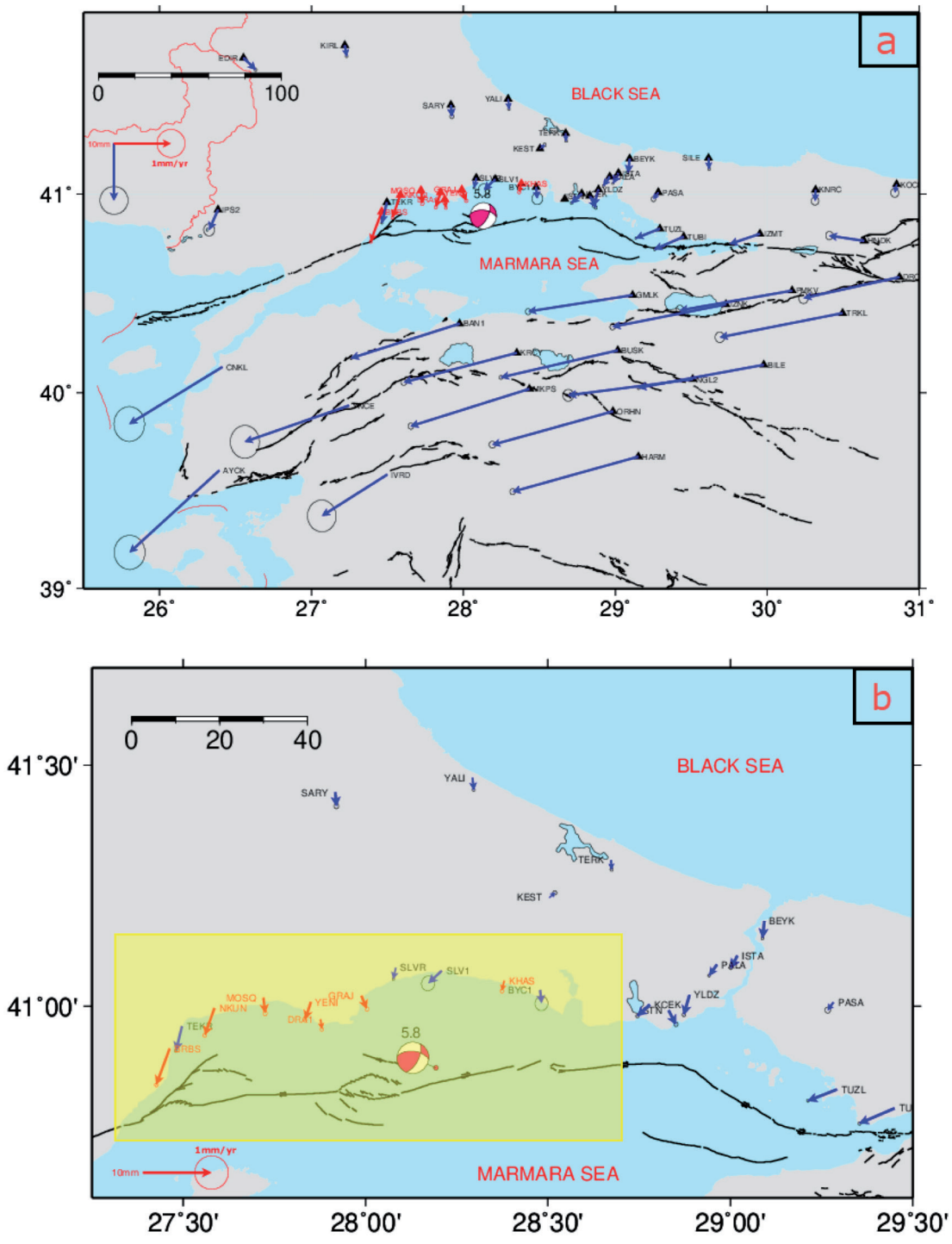


Fig. 4 - Horizontal velocity field for the whole Marmara region (a) and study area (yellow rectangle in panel b). The blue (40 pre-installed cGPS stations) and red (7 new cGPS stations) arrows are velocities and their uncertainties with respect to the Eurasia-fixed reference frame obtained from our first step analysis.

Additionally, strain analysis was performed with the GEODSUIT software using the estimated velocity field of the region. This software is used to analyse geodetic data in order to determine geodynamic parameters of tectonic phenomenon, such as plate motions, strain accumulations, crustal deformations and fault slip rates (Aktuğ *et al.*, 2010). The software uses the routines and methods given in Shen *et al.* (1996) and Aktuğ *et al.* (2009) to derive strain rates from the estimated station velocities. To explain more clearly, the strain rates for grid points are determined by translations and rotations according to the least-squares approach within this method. Uncertainties for the velocity field are given in Shen *et al.* (1996) as:

$$C_{ij} = Q_{ij} exp \frac{||r_x^r||^2 + ||r_y^r||^2}{\sigma_D^2} \quad (1)$$

where Q_{ij} is the covariance matrix of estimated velocities, σ_D^2 is the smoothing constant that acts as a spatial smoothing factor to define the contribution of nearby points to the strain rate parameters of each element and r_x^r and r_y^r are the position vectors for *x*- and *y*-axis, respectively (Aktuğ *et al.*, 2009). In this study, the grid interval setting of 10 km was introduced for the estimations of the strain rates.

Moreover, the software can provide inverse and forward modelling of displacements. The forward modelling approach follows the equations given in Okada (1985) for a finite fault definition. However, inverse modelling is also possible using surface displacements of a finite dislocation and fault geometry in an elastic half-space described in Okada (1985). The details of the optimisation strategy between fault geometry and surface displacements are presented in Aktuğ *et al.* (2010).

In this study, the strain rates were generated using the GEODSUIT software for the study area in the yellow rectangle (Fig. 5).

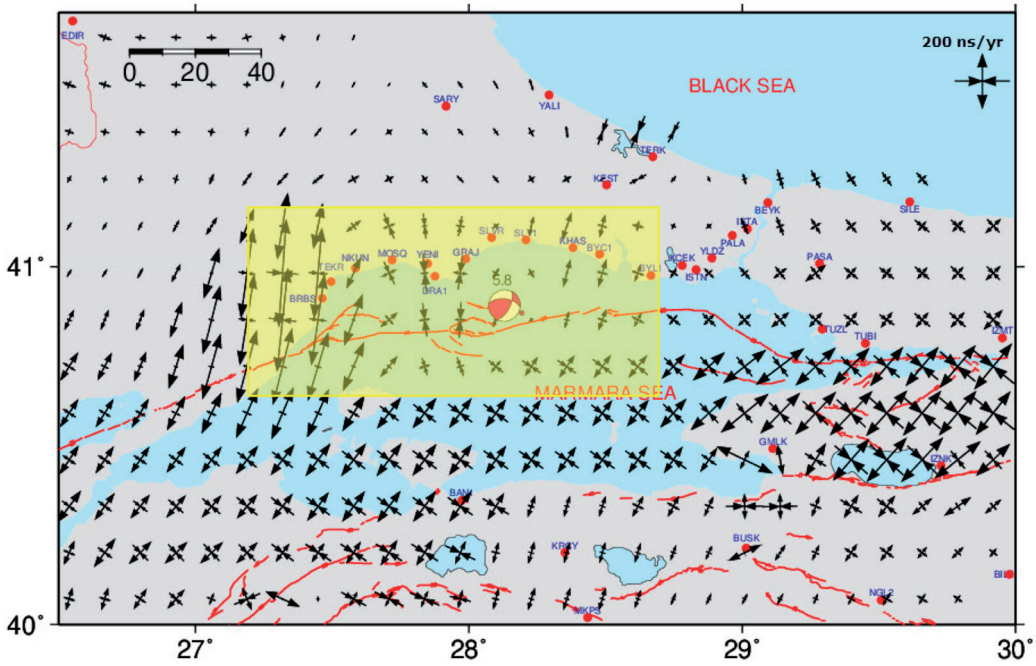


Fig. 5 - Strain rate map of the study area produced by GEODSUIT software. The yellow rectangle shows our study area. The focal mechanism represents the event occurring on 26 September 2019 (M_w = 5.8).

Fig. 5 demonstrates that the maximum deformations accumulating until the September 2019 earthquakes (KOERI, 2019) can be determined by analysing the data obtained from August 2017 to September 2019. Thus, it is understood that the geodetic network proposed by Klein *et al.* (2017) and designed for our study area has achieved its purpose. In addition, the geodetic data from this newly implemented network is scientifically valid for the central Marmara region and it was proven that the strain accumulations estimated for the inter-seismic period on mid-segments of the NAF after these earthquakes can be considered significant contributions to the literature.

3. Discussion and conclusions

A geodetic network was established to constrain the mid-segments of the NAF between Istanbul and Tekirdağ provinces. As a result of the successful network operation, it was possible to classify data acquisitions from cGPS stations into two data sets where the first stack covers approximately two years of data and the second contains more data than the other including two crucial earthquakes. Following this, two different GNSS data processing strategies were considered, either integrating the new geodetic data from our implementations into the whole data set or excluding it. Thus, strain analysis performed with the data set from Aktuğ *et al.* (2009) excluding the new geodetic data indicates that there are no significant deformations in the study area (Fig. 6a). On the contrary, by evaluating the new geodetic data set, strain accumulations are clearly seen in the western part of the central Marmara region (Fig. 6b). Thanks to the dense geodetic network with our new stations as shown in Fig. 2a, the strain estimations were evidently improved with the additional data set.

The strain analysis presented here demonstrates a significant difference in the deformation pattern of the study area depending on the enhancement of the geodetic network density. The statistical fundamentals for the results provided by the GEODSUIT software are referred to the detailed study published by Aktuğ *et al.* (2009).

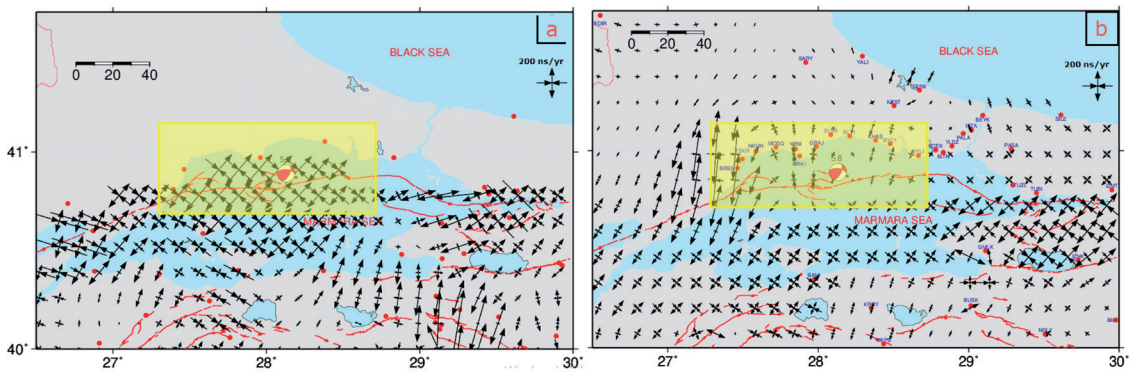


Fig. 6 - Strain rate maps for the study area without (a) and with (b) our geodetic data. Yellow rectangles represent our study area and can also be seen in Fig. 1.

This study ensures elimination of the deficiencies in Ergintav *et al.* (2014) caused by poor geodetic data close to the shoreline between the west of Istanbul and Tekirdağ provinces. It is clear that the geodetic network structure proposed in Klein *et al.* (2017) was confirmed with our

results from this study. Although Schmittbuhl *et al.* (2015) and Bulut *et al.* (2019) reported the sparse distribution of seismic activity on the KS, our study indicates ongoing but relatively less strain accumulations compared to western segments of the NAF. Therefore, different strategies based on marine geodesy or local dense seismological networks close to the KS could provide an explanation for this phenomenon.

As a result, it was understood that the new geodetic network is, and will be, very useful for monitoring crustal deformations in the central Marmara region of the NAF. According to our evaluation, the TS, KS, and CeS seem to be the most active sections of the NAF in the Sea of Marmara. In addition, it may be stated that seismic activities on the CeS transfer the stress to the TS and KS. However, in the framework of the literature, the forecasts about a probable destructive earthquake within the CiS contradict our evaluation. Since our project does not focus on the eastern Marmara region, our geodetic network is not dense enough to determine the strain accumulations in that region. It can, therefore, be said that our results could be improved with the implementations of denser cGPS stations for the eastern Marmara region. The KS of the NAF is stationary, which might indicate possible creeping or a locked fault. According to our evaluation, deformations are ongoing and may cause a major earthquake in that region. Even though the numerical results for the strain accumulations do need to be distinctly discussed and improved, we emphasise the ability of our new design network in handling recent geodetic data for probable earthquake forecasting in the region.

In conclusion, due to the enhanced spatial resolution of the geodetic data with our new implementations in the central Marmara region, the seismic risks in the region can be monitored in more detail and the results derived from this study can lead other studies concerning seismic hazard analysis.

Acknowledgements. We would like to thank all participants (Patrice Ulrich, Volkan Özbey, Turan Erden, Zafer Köse, Kayhan Aladoğan, Nurullah Şen, Melih Yamaç, Mehmet Atasoy) in this project who helped during the field study. In addition, we appreciate the great support of Tekirdağ Metropolitan, Çorlu and M.ereğlisi municipalities, CORS-TR, ISKI-UKBS and Fuat Agalday. The figures in this paper were produced using the public domain GMT software (Wessel and Smith, 1995). This research was supported by the Initiative d'Excellence (IDEX) funding framework (Université de Strasbourg), the Institut National des Sciences de l'Univers (INSU ALEAS) and Hitit University Scientific Research Projects Fund (ODMYO19001.15.002).

REFERENCES

Aksoy M.E.; 2009: *Active tectonics and paleoseismology of the Ganos Fault segment and seismic characteristics of the 9 August 1912 Mürefte earthquake of the North Anatolian Fault (western Turkey*). Ph.D. Thesis in Earth System Sciences, Istanbul Technical University, Eurasia Institute of Earth Sciences and University of Strasbourg, Institute de Physique du Globe, Strasbourg, 314 pp.

Aktuğ B., Nocquet J.M., Cingoz A., Parsons B., Erkan Y., England P., Lenk O., Gurdal M.A., Kılıçoğlu A., Akdeniz H. and Tekgül A.; 2009: *Deformation of western Turkey from a combination of permanent and campaign GPS data: limits to block-like behavior*. J. Geophys. Res.: Solid Earth, 114, B10404, doi: 10.1029/2008JB006000.

Aktuğ B., Kaypak B. and Çelik R.N.; 2010: *Source parameters of 03 February 2002 Çay earthquake, Mw 6.6 and aftershocks from GPS data, southwestern Turk*ey. J. Seismol., 14, 445-456.

Aktuğ B., Doğru A., Özener H. and Peyret M.; 2015: *Slip rates and locking depth variation along central and easternmost segments of North Anatolian Fault*. Geophys. J. Int., 202, 2133-2149, doi: 10.1093/gji/ggv274.

Ambraseys N.N.; 1970: *Some characteristic features of the North Anatolian Fault zone*. Tectonophys., 9, 143-165.

Ambraseys N.N.; 2002: *The seismic activity of the Marmara Sea region over the last 2000 years*. Bull. Seismol. Soc. Am., 92, 1-18.

Armijo R., Meyer B., Navarro S. and King G.; 2002: *Slip partitioning in the Sea of Marmara pull-apart: a clue to propagation processes of the North Anatolian Fault*. Terra Nova, 14, 80-86.

Barka A.; 1992: *The North Anatolian Fault zone*. Ann. Tectonicae, 6, 164-195.

Barka A.; 1996: *Slip distribution along the North Anatolian Fault associated with the large earthquakes of the period 1939 to 1967*. Bull. Seismol. Soc. Am., 86, 1238-1254.

Bulut F., Aktuğ B., Yaltırak C. and Özener H.; 2019: *Magnitudes of future large earthquakes near Istanbul quantified from 1500 years of historical earthquakes, present-day microseismicity and GPS slip rates*. Tectonophys., 764, 77-87, doi: 10.1016/j.tecto.2019.05.005.

Çakir Z., Akoglu A.M., Belabbes S., Ergintav S. and Meghraoui M.; 2005: *Creeping along the Ismetpasa section of the North Anatolian Fault (western Turkey): rate and extent from InSAR*. Earth Planet. Sci. Lett., 238, 225-234.

Çırmık A. and Pamukçu O.; 2017: *Clarifying the interplate main tectonic elements of western Anatolia, Turkey by using GNSS velocities and Bouguer gravity anomalies*. J. Asian Earth Sci., 148, 294-304.

Çırmık A., Pamukçu O., Gönenç T., Kahveci M., Şalk M. and Herring T.; 2016: *Examination of the kinematic structures in İzmir (western Anatolia) with repeated GPS observations (2009, 2010 and 2011)*. J. Afr. Earth Sci., 126, 1-12, doi: 10.1016/j.jafrearsci.2016.11.020.

Emre Ö., Duman T.Y., Özalp S., Elmacı H., Olgun Ş. and Şaroğlu F.; 2013: *Active fault map of Turkey with and explanatory text.* General Directorate of Mineral Research and Exploration, Ankara, Turkey, Special Publication Series, Vol. 30, 95 pp.

Ergintav S., Reilinger R.E., Çakmak R., Floyd M., Çakir Z., Doğan U. and Özener H.; 2014: *Istanbul's earthquake hot spots: geodetic constraints on strain accumulation along faults in the Marmara seismic gap*. Geophys. Res. Lett., 41, 5783-5788.

Floyd M.A., Billiris H., Paradissis D., Veis G., Avallone A., Briole P., McClusky S., Nocquet J.-M., Palamartchouk K., Parsons B. and England P.C.; 2010: *A new velocity field for Greece: implications for the kinematics and dynamics of the Aegean.* J. Geophys. Res.: Solid Earth, 115, B10403, doi: 10.1029/2009JB007040.

Herring T.A., King R.W. and McClusky S.C.; 2010: *Introduction to GAMIT/GLOBK, Release 10.4.* Massachusetts Institute of Technology, Department of Earth, Atmospheric, and Planetary Sciences, Cambridge, MA, USA, 48 pp.

Jackson J. and McKenzie D.P.; 1984: *Active tectonics of Alpine - Himalayan Belt between western Turkey and Pakistan*. Geophys. J. R. Astron. Soc., 77, 185-264.

Kandilli Observatory and Earthquake Research Institute (KOERI); 2019: *24 and 26 September 2019 Earthquakes' information, (24 eylül 2019 silivri açiklari-istanbul (marmara denizi) depremi basin bülteni ve 26 eylül 2019 silivri açiklari-istanbul (marmara denizi) depremi basin bülteni)*, in Turkish.

Kaneko Y., Fialko Y., Sandwell D.T., Tong X. and Furuya M.; 2013: *Interseismic deformation and creep along the central section of the North Anatolian Fault (Turkey): InSAR observations and implications for rate and state friction properties*. J. Geophys. Res.: Solid Earth, 118, 316-331, doi: 10.1029/2012JB009661.

Ketin I.; 1948: *Uber die tektonisch-mechanischen folgerungen aus den grossen anatolischen erdbeben des letzten dezenniums*. Geol. Rund., 36, 77-83.

Klein E., Duputel Z., Masson F., Yavaşoğlu H. and Agram P.; 2017: *Aseismic slip and seismogenic coupling in the Marmara Sea: what can we learn from onland geodesy*? Geophys. Res. Lett., 44, 3100-3108.

Kutoglu H.S., Akcin H., Kemaldere H. and Gormus K.H.; 2008: *Triggered creep rate on the Ismetpasa segment of the North Anatolian Fault*. Nat. Hazards Earth Syst. Sci., 8, 1369-1373.

Le Pichon X., Chamot-Rooke N., Rangin C. and Sengör A.M.C.; 2003: *The North Anatolian Fault in the Sea of Marmara*. J. Geophys. Res.: Solid Earth, 108(B4), 2179, doi: 10.1029/2002JB001862.

Le Pichon X., İmren C., Rangin C., Şengör A.M.C. and Siyako M.; 2014: *The South Marmara Fault*. Int. J. Earth Sci., 103, 219-231, doi: 10.1007/s00531-013-0950-0.

McClusky S., Balassanian S., Barka A., Demir C., Ergintav S., Georgiev I., Gurkan O., Hamburger M., Hurst K., Kahle H., Kastens K., Kekelidze G., King R., Kotzev V., Lenk O., Mahmoud S., Mishin A., Nadriya M., Ouzounis A., Paradissis D., Peter Y., Prilepin M., Reilinger R., Şanlı I., Seeger H., Tealeb A., Toksöz M.N. and Veis G.; 2000: *Global Positioning System constraints on plate kinematics and dynamics in the eastern Mediterranean*. J. Geophys. Res.: Solid Earth, 105, 5695-5719.

McKenzie D.P.; 1972: *Active tectonics of the Mediterranean region*. Geophys. J. R. Astron. Soc., 30, 109-185, doi: 10.1111/j.1365-246X.1972.tb02351.x.

Meghraoui M., Aksoy M.E., Akyüz H.S., Ferry M., Dikbas A. and Altunel E.; 2012: *Paleoseismology of the North Anatolian Fault at Güzelköy (Ganos segment, Turkey): size and recurrence time of earthquake ruptures west of the Sea of Marmara.* Geochem. Geophys. Geosyst., 13, Q04005, doi: 10.1029/2011GC003960.

Nyst M. and Thatcher W.; 2004: *New constraints on the active tectonic deformation of the Aegean*. J. Geophys. Res.: Solid Earth, 109, B11406.

Okada Y.; 1985: *Surface deformation due to shear and tensile faults in a half-space*. Bull. Seismol. Soc. Am., 75, 1135-1154.

Ozdemir S. and Karslıoğlu M.O.; 2019: *Soft clustering of GPS velocities from a homogeneous permanent network in Turkey*. J. Geod., 93, 1171-1195, doi: 10.1007/s00190-019-01235-z.

Özener H., Arpat E., Ergintav S., Dogru A., Çakmak R., Turgut B. and Doğan U.; 2010: *Kinematics of the eastern part of the North Anatolian Fault zon*e. J. Geodyn., 49, 141-150, doi: 10.1016/j. jog.2010.01.003.

Poyraz F., Hastaoğlu K.O., Koçbulut F., Tiryakioğlu İ., Tatar O., Demirel M., Duman H., Aydın C., Ciğer A.F., Gursoy O., Turk T. and Sıgırcı R.; 2019: *Determination of the block movements in the eastern section of the Gediz Graben (Turkey) from GNSS measurements*. J. Geodyn., 123, 38-48, doi: 10.1016/j.jog.2018.11.001.

Reilinger R., McClusky S., Vernant P., Lawrence S., Ergintav S., Çakmak R., Özener H., Kadirov F., Guliev I., Stepanyan R., Nadariya M., Hahubia G., Mahmoud S., Sakr K., ArRajehi A., Paradissis D., Al-Aydrus A., Prilepin M., Guseva T., Evren E., Dmitrotsa A., Filikov S.V., Gomez F., Al-Ghazzi R. and Karam G.; 2006: *GPS constraints on continental deformation in the Africa - Arabia, Eurasia continental collision zone and implications for the dynamics of plate interactions*. J. Geophys. Res.: Solid Earth, 111, B05411.

Schmittbuhl J., Karabulut H., Lengline O. and Bouchon M.; 2015: *Seismicity distribution and locking depth along the main Marmara Fault, Turkey*. Geochem. Geophys. Geosyst., 17, 954-965, doi: 10.1002/2015GC006120.

Schmittbuhl J., Karabulut H., Lengliné O. and Bouchon M.; 2016: *Long-lasting seismic repeaters in the central basin of the main Marmara Fault*. Geophys. Res. Lett., 43, 9527–9534, doi: 10.1002/2016GL070505.

Şengör A.M.C., Tüysüz O., İmren C., Sakınc M., Eyidoğan H., Görür N., Le Pichon X. and Rangin C.C.; 2004: *The North Anatolian Fault: a new look.* Annu. Rev. Earth Planet. Sci., 33, 1-75.

Shen Z.-K., Jackson D.D. and Ge X.B.; 1996: *Crustal deformation across and beyond the Los Angeles basin from geodetic measurements*. J. Geophys. Res.: Solid Earth, 101, 27957-27980.

Tatar O., Poyraz F., Gursoy H., Çakir Z., Ergintav S., Akpinar Z., Koçbulut F., Sezen F., Turk T., Hastaoğlu O., Polat A., Mesci B.L., Gursoy O., Ayazli E., Çakmak R., Belgen A. and Yavaşoğlu H.; 2012: *Crustal deformation and kinematics of the eastern part of the North Anatolian Fault zone (Turkey) from GPS measurements*. Tectonophys., 518-521, 55-62, doi: 10.1016/j.tecto.2011.11.010.

Tiryakioğlu I.; 2013: *Geodetic aspects of the 19 May 2011 Simav Earthquake in Turkey.* Geomatics, Nat. Hazards Risk, 6, 76-89, doi: 10.1080/19475705.2013.831379.

Tiryakioğlu I., Floyd M., Erdoğan S., Gülal E., Ergintav S., McClusky S. and Reilinger R.; 2013: *GPS constraints on active deformation in the Isparta Angle region of SW Turkey*. Geophys. J. Int., 195, 1455-1463.

Tiryakioğlu I., Yiğit C.O., Yavaşoğlu H., Saka M.H. and Alkan R.M.; 2017: *The determination of interseismic, coseismic and postseismic deformations caused by the Gökçeada - Samothraki earthquake (2014, Mw: 6.9) based on GNSS data*. J. Afr. Earth Sci., 133, 86-94.

Tiryakioğlu I., Aktuğ B., Yiğit C.Ö., Yavaşoğlu H., Sözbilir H., Özkaymak Ç., Poyraz F., Taneli E., Bulut F., Doğru A. and Özener H.; 2018: *Slip distribution and source parameters of the 20 July 2017 Bodrum - Kos earthquake (Mw 6.6) from GPS observations*. Geodinamica Acta, 30, 1-14.

Wessel P. and Smith W.H.F; 1995: *New version of the generic mapping tools released*. EOS Trans. Amer. Geophys. Union, 76, 329, doi: 10.1029/95EO00198.

Yaltırak C.; 2002: *Tectonic evolution of the Marmara Sea and its surrounding*s. Mar. Geol., 190, 493-529.

Yavaşoğlu H., Tarı E., Tüysüz O., Çakır Z. and Ergintav S.; 2011: *Determining and modeling tectonic movements along the central part of the North Anatolian Fault (Turkey) using geodetic measurements*. J. Geodyn., 51, 339-343.

Corresponding author: Hasan Hakan Yavaşoğlu
ITU, Geomatic Eng. Dept.
Maslak, Istanbul, Turkey
Phone: +90 212 2853829; e-mail: yavasoglu@itu.edu.tr